Spectrochimica Acta Part A: Molecular and Biomolecular Spectroscopy 242 (2020) 118723

Contents lists available at ScienceDirect

Spectrochimica Acta Part A: Molecular and Biomolecular Spectroscopy

journal homepage: www.elsevier.com/locate/saa

Characterization of Kemer L4 meteorite using Raman spectroscopy, X-ray diffraction, magnetization measurements and Mössbauer spectroscopy

A.A. Maksimova [a], E.V. Petrova [a], A.V. Chukin [a], M.S. Karabanalov [b], B.A. Nogueira [c], R. Fausto [c], M. Yesiltas [d], I. Felner [e], M.I. Oshtrakh [a,*]

[a] Institute of Physics and Technology, Ural Federal University, Ekaterinburg 620002, Russian Federation
[b] Institute of Material Science and Metallurgy, Ural Federal University, Ekaterinburg 620002, Russian Federation
[c] CQC, Department of Chemistry, University of Coimbra, 3004-535 Coimbra, Portugal
[d] Faculty of Aeronautics and Space Sciences, Kirklareli University, Kirklareli, Turkey
[e] Racah Institute of Physics, The Hebrew University, Jerusalem, Israel

ARTICLE INFO

Article history:
Received 13 April 2020
Received in revised form 6 July 2020
Accepted 12 July 2020
Available online 20 July 2020

Keywords:
Kemer L4 ordinary chondrite
X-ray diffraction
Raman spectroscopy
Magnetization measurements
Mössbauer spectroscopy

ABSTRACT

The bulk interior of Kemer L4 ordinary chondrite was characterized for the first time by means of optical microscopy, scanning electron microscopy with energy dispersive spectroscopy, Raman spectroscopy, X-ray diffraction, magnetization measurements and Mössbauer spectroscopy with a high velocity resolution. The main and minor iron-bearing phases were found as well as ferrihydrite as a result of weathering. The Fe^{2+} partitioning among the M1 and M2 sites in olivine, orthopyroxene and clinopyroxene was determined from the X-ray diffraction. The ratios of Fe^{2+} occupancies for these crystals were estimated from both X-ray diffraction and Mössbauer spectroscopy data and appeared to be in a good agreement. The distribution coefficients K_D and the temperatures of equilibrium cation distribution T_{eq} were also evaluated for olivine and orthopyroxene from two independent techniques and were in a good consistence: $K_D = 1.77$, $T_{eq} = 441$ K (X-ray diffraction) and $K_D = 1.77$, $T_{eq} = 439$ K (Mössbauer spectroscopy) for olivine and $K_D = 0.10$, $T_{eq} = 806$ K (X-ray diffraction) and $K_D = 0.09$, $T_{eq} = 787$ K (Mössbauer spectroscopy) for orthopyroxene. The fusion crust of Kemer L4 was studied using X-ray diffraction, magnetization measurements and Mössbauer spectroscopy. Magnesioferrite and probably maghemite were found in the fusion crust in addition to other phases observed in the bulk interior.

1. Introduction

The majority of all meteorites reached the Earth are ordinary chondrites (~80%). Ordinary chondrites, as the main part of stony meteorites, were classified as undifferentiated meteorites [1]. This group of meteorites was formed together with the Solar System and brings information about early stage of its formation as well as about further transformation of matter in space including information about its shock and thermal history. Therefore, study of ordinary chondrites using various physical techniques is of interest.

Ordinary chondrites consist of the following iron-bearing crystals: olivine (Fe, Mg)$_2$SiO$_4$, orthopyroxene (Fe, Mg)SiO$_3$, clinopyroxene (Fe, Mg, Ca)SiO$_3$, troilite FeS, chromite FeCr$_2$O$_4$, hercynite FeAl$_2$O$_4$, ilmenite FeTiO$_3$, grains of Fe-Ni-Co alloy in the form of α-Fe(Ni, Co), α$_2$-Fe(Ni, Co), γ-Fe(Ni, Co) and γ-FeNi phases as well as some ferric compounds resulting from terrestrial weathering. There are also iron-free crystals in ordinary chondrites from albite NaAlSi$_3$O$_8$ to anorthite CaAl$_2$Si$_2$O$_8$. Details of ordinary chondrites composition and classification can be found in [2,3].

The Kemer meteorite fell around noon on March 3, 2008 in the province of Mugla, Turkey, near Kemer town (36°32′31″ N, 29°25′05.6″ E). Three stones (fully fusion crusted) were recovered and subsequently classified as an ordinary chondrite from group L and petrological type 4, with shock stage S4/5 and weathering grade W0 (at that time). Average values of fayalite Fa (a molar fraction of Fe$_2$SiO$_4$ in olivine solid solution of Fe$_2$SiO$_4$–Mg$_2$SiO$_4$) and ferrosilite Fs (a molar fraction of FeSiO$_3$ in orthopyroxene solid solution of FeSiO$_3$–MgSiO$_3$) are 24 mol% and 19 mol%, respectively (Meteoritical Bulletin, No 99, 2012). Hitherto, Kemer meteorite has not been characterized by physical techniques, while these techniques are very useful in the studies of ordinary chondrites, for example, X-ray diffraction (XRD), *e.g.* [4–6], Raman spectroscopy, *e.g.* [7,8], magnetization measurements, *e.g.* [9] and ^{57}Fe Mössbauer spectroscopy, *e.g.* [10,11]. Therefore, we present here results obtained for one Kemer L4 fragment with the fusion crust by means of optical microscopy, scanning electron microscopy (SEM) with energy dispersive spectroscopy (EDS), Raman spectroscopy, XRD, magnetization measurements and ^{57}Fe Mössbauer spectroscopy.

* Corresponding author.
E-mail address: oshtrakh@gmail.com (M.I. Oshtrakh).

https://doi.org/10.1016/j.saa.2020.118723
1386-1425/

2. Materials and methods

A piece of Kemer L4 with the fusion crust was cut off (Fig. 1) and delivered from Kirklareli, Turkey to Ekaterinburg, Russian Federation for samples preparation for further analysis in the laboratories involved in this study. The polished section of this sample was prepared by the standard method for characterization using optical microscopy, SEM with EDS and Raman spectroscopy. Then, a thin powder was prepared from this surface for XRD, magnetization measurements and Mössbauer spectroscopy of the bulk interior of Kemer L4. About 200 mg of the sample powder was used for XRD, while only few mg of that were used for magnetization measurements. The sample for Mössbauer spectroscopy was prepared with a thickness of ~6 mg Fe/cm^2, by gluing the sample powder on Al foil free from Fe with a diameter of 20 mm. A part of the fusion crust thin layer was removed from the piece and powdered. This powder was used for XRD, magnetization measurements and Mössbauer spectroscopy, the samples for these techniques being prepared as described above for the bulk interior powder.

At the Ural Federal University (Ekaterinburg), characterization of Kemer L4 was done by optical microscopy under the non-polarized and polarized reflected light, using an Axiovert 40 MAT microscope (Carl Zeiss), and by scanning electron-ion microscopy, using an Auriga CrossBeam (Carl Zeiss) microscope with an accelerating potential of 20 kV and a probe current of 200 μA, coupled with an EDS device X-max 80 (Oxford Instruments), for analysis of chemical composition.

At the University of Coimbra (Coimbra), the Raman spectra were collected using a Horiba LabRam HR Evolution micro-Raman system, with laser excitation at 532 nm, a laser power of ~5 mW, spectral resolution 1.5 cm^{-1}, spot size ~1 μm and a 50× magnification lens (NA = 0.75). The Raman spectra were collected with an acquisition time of 5 to 10 s, and 5 to 10 accumulations. The Raman map was obtained for a 94×118 μm^2 area, with spectra being collected using a grid of 3×3 μm^2.

XRD analyses of the bulk interior and fusion crust powdered samples were done at the Ural Federal University (Ekaterinburg) using an XRD–7000 powder diffractometer (Shimadzu) operating at 40 kV and 30 mA with CuK_α radiation using a monochromator. Scanning was performed over 2Θ from 13° to 86°, with a step of 0.03° per 10 s. XRD patterns were processed using the Panalytical X'Pert High Score Plus (version 2.2c) software. The X-ray data were fitted by the least squares procedure using the Rietveld full profile refinements program. This Rietveld implementation is based on the source code of the modified version of the LHPM program [12]. The least squares refinements were performed with pseudo Voigt peak profiles. The phase composition was evaluated using the ICDD PDF-2 database. Then, initial structural parameters, atomic positions and temperature factors for the refinements were taken from the ICSD database. The quality of the refinement was evaluated by indices characterizing the fitting model: $R_P = 2.4$; $R_{WP} = 3.2$; $R_{EXP} = 1.9$; GOF (goodness of fit) = 2.8, whose values demonstrate its good quality, which allows an estimation of phase compositions up to the first decimal digit.

Fig. 1. Photograph of Kemer L4 piece used in the study showing the interior and the fusion crust.

At the Hebrew University (Jerusalem), magnetization measurements were carried out using a commercial SQUID magnetometer MPMS-5S (Quantum Design) in the temperature range 5–295 K. The differential SQUID sensitivity was 10^{-7} emu. The samples were cooled to 5 K and the fields were switched on to trace the zero-field-cooled (ZFC) branches of the magnetization $M(T)$ curves. The magnetometer was adjusted to be in a real $H = 0$ state prior to recording the ZFC curves. Under this field, the field-cooled (FC) $M(T)$ branches were measured *via* heating from 5 to 295 K. The fields up to 50 kOe at 5 and 295 K were applied for isothermal magnetization $M(H)$ curves measurements.

^{57}Fe Mössbauer spectra were measured at the Ural Federal University (Ekaterinburg) using an automated precision Mössbauer spectrometric system developed in-house based on the SM-2201 spectrometer, with a saw-tooth shape velocity reference signal formed by a digital-analog converter using discretization of 2^{12}, resulting in a velocity quantification in 4096 steps. The high discretization level of the velocity scale provides much better adjustment to resonance, and significantly increases the spectra quality and analytical possibilities of Mössbauer spectroscopy but increases the measurement time. Details and characteristics of this spectrometer and the system were described in [13–16]. The 1.8×10^9 Bq ^{57}Co(Rh) source (Ritverc GmbH, St. Petersburg) was used at room temperature. The Mössbauer spectra of Kemer L4 samples were measured in transmission geometry with moving absorber at 295 K and recorded in 4096 channels. Then, these spectra were converted into 1024-channel spectra, by a consequent summation of four neighboring channels, to increase the signal-to-noise ratio for the minor spectral components. Statistics in the obtained spectra of the bulk interior and the fusion crust was ~12.5×10^6 and ~7.4×10^6 counts per channels, and the signal-to-noise ratio was 241 and 233, respectively. Each spectrum was measured over a period of 2–3 weeks, to reach appropriate signal-to-noise ratio for reliable fits.

Mössbauer spectra were computer-fitted with the least square procedure using UNIVEM-MS program with a Lorentzian line shape. The line shape of the 1024-channel Mössbauer spectrum of the reference absorber of α-Fe foil with a thickness of 7 μm was pure Lorentzian, with line widths (Γ, the full width at a half maximum) of $\Gamma_{1,6} = 0.238 \pm 0.031$ mm/s, $\Gamma_{2,5} = 0.232 \pm 0.031$ mm/s and $\Gamma_{3,4} = 0.224 \pm 0.031$ mm/s for the 1st and the 6th, the 2nd and the 5th, and the 3rd and the 4th peaks in the measured sextet, respectively. The velocity resolution (velocity per one channel) in the 1024-channel Mössbauer spectra was ~0.015 mm/s per channel for the meteorite bulk interior and ~0.019 mm/s per channel for its fusion crust. Spectral parameters such as isomer shift, δ, quadrupole splitting/quadrupole shift for magnetically split components, $\Delta E_Q/\varepsilon$ ($2\varepsilon = \Delta E_Q$), magnetic hyperfine field, H_{eff}, line width, Γ, relative subspectrum (component) area, A, and normalized statistical quality of the fit, χ^2, were determined.

For the most reliable fits of the measured spectra, we used a new model that takes into account the spectral components related to the ^{57}Fe in the crystallographically non-equivalent M1 and M2 sites in olivine, orthopyroxene and clinopyroxene, and components related to metallic iron α-, α_2- and γ-phases with variations in Ni concentration, chromite, hercynite and ferric compounds. Moreover, for the Mössbauer spectrum of the bulk interior sample of Kemer L4, a simulation of the full static Hamiltonian was applied for the troilite subspectrum fit. The latter results in more reliable Mössbauer parameters for the minor spectral components and overcomes the problem with fitting the troilite FeS component using the full static Hamiltonian in the complex Mössbauer spectra of ordinary chondrites (see [17,18] and references therein). The new fitting model was described and compared with the full static Hamiltonian fit in [19] and applied recently for various ordinary chondrites spectra re-fitting in [20] without more detailed analysis of the

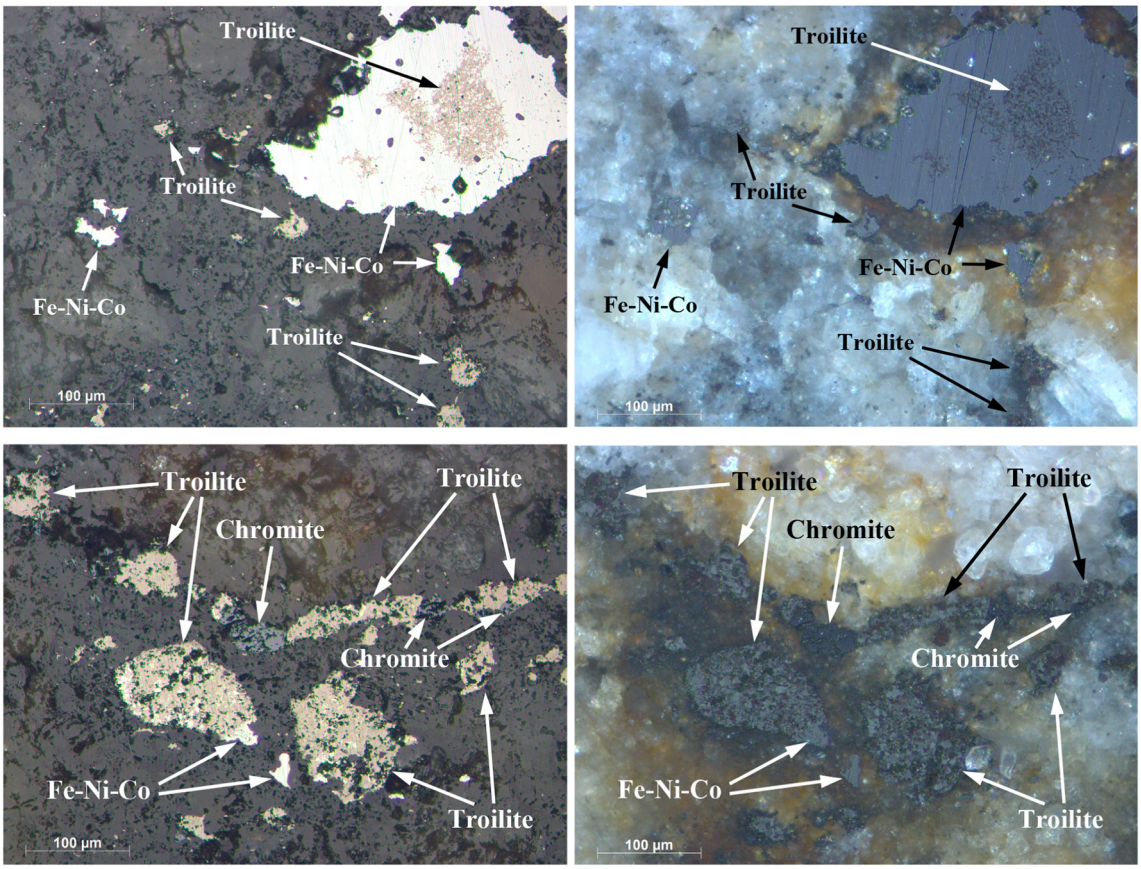

Fig. 2. Selected optical microscopy images of Kemer L4 polished section done under the non-polarized and polarized light with indication of some phases.

presence of minor iron-bearing phases. Further, this model was successfully used for detailed studies of some ordinary chondrites in [21–23]. Criteria determining the best fit solution were the differential spectrum (the difference between experimental and calculated spectral points), χ^2 and the physical meaning of the parameters.

The instrumental (systematic) error for each spectral point was equivalent to ±0.5 channel (in the velocity scale), that for the hyperfine parameters was equivalent to ±1 channel (in mm/s or kOe). If an error calculated with the fitting procedure (fitting error) for these parameters exceeded the instrumental (systematic) error, the larger error was used instead. The values of *A* are given in tables as calculated in the fit with two decimal digits to keep the total relative area equal to 100%. The estimated relative error for *A* usually did not exceed 10%. Values of δ are given relative to α-Fe at 295 K.

3. Results and discussion

3.1. The bulk interior

Selected images of the Kemer L4 polished section obtained using optical microscopy under non-polarized and polarized light are shown in Fig. 2. These images demonstrate a typical ordinary chondrite texture with metal grains (Fe-Ni-Co alloy), and troilite and chromite inclusions within the silicate matrix consisting of olivine and orthopyroxene. There

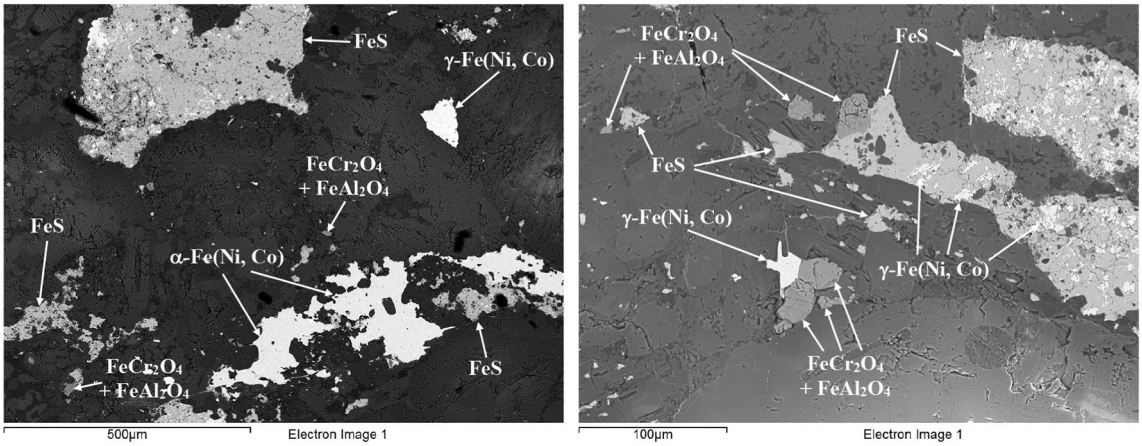

Fig. 3. Selected scanning electron microscopy images of Kemer L4 polished section taken at different magnifications. Indicated phases were determined using energy dispersive spectroscopy.

Table 1
Averaged ranges of metal content in selected minor iron-bearing phases in the bulk interior of Kemer L4 ordinary chondrite obtained using energy dispersive spectroscopy.

Minor phases	Metal content, at%
α-Fe(Ni, Co)	
Fe	92.1–95.7
Ni	3.9–7.4
Co	0.2–1.1
α_2-Fe(Ni, Co)	
Fe	85.2
Ni	14.2
Co	0.6
γ-Fe(Ni, Co)	
Fe	45.7–58.7
Ni	41.1–54.0
Co	0.1–0.3
Paramagnetic γ-Fe(Ni, Co)	
Fe	69.3–70.2
Ni	29.4–30.5
Co	0.2–0.6
FeS	
Fe	48–49
S	51–52
$FeCr_2O_4$	
Fe	10.0–12.5
Cr	17.7–21.9
Al	2.2–2.7
Ti	0.4–0.7
Mg	1.0–3.7

are various metal-troilite associations seen at the section plane, some of them show the presence of fine-grained troilite inside the metal grain and *vice-versa*.

Selected SEM images with different magnification of the Kemer L4 polished section are shown in Fig. 3. It is clearly seen that troilite grains contain numerous fine-grained metal inclusions. The metal content (in percentage of atoms; at.%) in selected phases is given in Table 1. The presence of Al as the third metal in chromite indicates the possible presence of hercynite associated with chromite resulting from Cr substitution by Al. However, in one chromite grain only a large amount of Mg as the third metal was observed. Similar presence of Mg in chromite was recently detected in the stony part of Seymchan main group pallasite, which was considered as indication of the presence of magnesiochromite $Fe_{1-x}Mg_xCr_2O_4$ in addition to chromite in that meteorite [24]. However, in the case of Kemer L4, the presence of one chromite particle only with a large Mg content indicates that the total amount of magnesiochromite in the sample cannot be detected by XRD and Mössbauer spectroscopy, while hercynite content is enough for detection by these techniques. The content of Fe and S in troilite is close to stoichiometry. EDS analysis indicated the presence of α-Fe(Ni, Co) and γ-Fe(Ni, Co) phases in the metal grains. It was interesting to find metal grains with Ni content higher than 50 at.%. Several Fe-Ni-Co grains consist of a complex mixture of α-Fe (Ni, Co) and γ-Fe(Ni, Co) phases (Fig. 4), clearly demonstrating a variation of Ni content even within the same phase.

Representative Raman spectra of the Kemer L4 polished section are shown in Fig. 5 (top panels), conforming to olivine and orthopyroxene. A Raman mapping of a $94 \times 118\ \mu m^2$ area of the sample (corresponding to around 1200 different Raman spectra) is shown in the figure (bottom, right image) and highlights these two types of materials in green and red colors, respectively. This map allows to establish an easy correlation between the olivine and orthopyroxene rich regions of the sample with the optical microscope image also presented in the figure (bottom, left picture). In the spectrum of olivine, the observed strong doublet ascribable to the Si—O symmetric and anti-symmetric stretching vibrations, has peak positions at 823.3 and 855.4 cm^{-1}, while minor bands are observed at 606, 586, 543, 434, 419, 337, 333 and 303 cm^{-1}. All these bands fit well the spectra of forsterite [25–27] indicating the forsterite/fayalite ratio of $(70 \pm 3):(30 \pm 3)$ for Kemer L4. This ratio is comparable with the Fa values range of 23–25 mol% given in *Meteoretical Bulletin*, 99, 2012. The observed Raman spectrum of orthopyroxene shows the bands due to the Si—O stretching modes at 1009 and 1026 cm^{-1}, those due to the Si—O bending modes at 661 and 681 cm^{-1}, and that ascribable to the M—O stretching vibrations at 338 cm^{-1}. According to [28], these numbers correspond to a composition of the orthopyroxene with an enstatite/ferrosilite ratio of approximately from 87:13 to 80:20, *i.e.*, Fs is between 13 and 20 mol%, which is consistent with the value of Fs = 19 mol% for Kemer L4 given in *Meteoritical Bulletin*, 99, 2012.

The XRD pattern for the bulk interior of Kemer L4, with indication of selected reflections, is shown in Fig. 6. The Rietveld analysis showed the presence of the following phases in this sample: 53.2 wt% olivine (ICDD 01-080-1630), 22.6 wt% orthopyroxene (ICDD 01-083-0666), 7.3 wt% anorthite (ICDD 01-079-1149), 6.7 wt% Ca-rich clinopyroxene (ICDD 01-083-0088), 4.4 wt% α-Fe(Ni, Co) phase (ICDD 00-037-0474), 3.8 wt% troilite (ICDD 01-080-1030), 0.7 wt% γ-Fe(Ni, Co) phase (ICDD 01-089-4185), 0.6 wt% chromite (ICDD 00-034-0140), 0.2 wt% hercynite (ICDD 00-034-0192) and 0.5 wt% ferric compound in the form of ferrihydrite $5Fe_2O_3 \times 9H_2O$ (ICDD 00-046-1315). The unit cell parameters in silicate crystals in the bulk interior of Kemer L4 were determined by the Rietveld full profile analysis: $a = 10.268(4)$ Å, $b = 6.009(4)$ Å, $c = 4.772(3)$ Å for olivine, $a = 18.280(6)$ Å, $b = 8.862(5)$ Å, $c = 5.199(5)$ Å for orthopyroxene and $a = 9.76(5)$ Å, $b = 8.89(4)$ Å, $c = 5.28(3)$ Å, $\beta = 106.25°$ for Ca-rich clinopyroxene.

Fig. 7 shows the ZFC and FC plots of the bulk interior of Kemer L4 measured at 1 kOe and temperature varied from 5 to 295 K. The two branches show a moderate increase at low temperatures, indicating the presence of a tiny amount of a paramagnetic extra phase. In addition, two anomalies are observed: (i) a pronounced peak at $T \approx 62$ K and a small bulge at $T \approx 52$ K in the ZFC branch (see inset in Fig. 7, ZFC-FC plot), and a break in the FC one in the same temperature region; (ii) both ZFC and FC plots increase sharply till a bump around 200 K and further up to 260 K, and then start to decrease for higher temperatures. They do not merge at 295 K.

The origin of the peaks at around $T \approx 62$ K and $T \approx 52$ K is related to the ferrimagnetic chromite. It was demonstrated earlier that the ferrimagnetic-paramagnetic phase transition in chromate is in the temperature range 40–80 K [29]. However, in contrast to our previous studies of Northwest Africa 6286 LL6, Northwest Africa 7857 LL6 and Ozerki L6 ordinary chondrites, which demonstrated only one peak at around 60 K associated with chromite [21,23], there are two peaks observed for the bulk interior of Kemer L4. On the other hand, this looks like ZFC-FC plots for Annama H5 ordinary chondrite in the temperature range ~40–80 K [30]. It is possible that the observation of two peaks associated with two magnetic phase transitions is related to small variations in the accessory metals like Mg and Ti (see Table 1) in chromite inclusions (see also [29]).

A sharp increase of the magnetization up to T ~260 K is clearly seen in Fig. 7. This means that the magnetic transition temperature for the bulk interior of Kemer L4 is well above 300 K, as indicated clearly by the isothermal magnetization $M(H)$ curves described hereafter.

The two $M(H)$ curves measured at 5 and 295 K first increase up to 4–5 kOe, tends to saturate up to 50 kOe at 5 K but almost saturated (at 5 kOe) at 295 K. No hysteresis is observed in both plots. Due to the presence of a paramagnetic fraction, which dominates at low temperatures, the experimental $M(H)$ plot at 5 K clearly reveals this admixture of magnetic and paramagnetic components and can be fitted as: $M(H)_{exp} = M_S + (\chi_p H)$, where the saturation moment M_S is the intrinsic magnetic phase contribution, and $\chi_p H$ is the linear paramagnetic contribution. This procedure yields $M_S = 33.9$ and 31.1 emu/g for $T = 5$ and 295 K, respectively. The observed small decrease (around 10%) upon increase of temperature confirms our statement that the magnetic transition of sample takes place at a temperature much higher than room temperature. This picture is also consistent with the Mössbauer data presented below.

The Mössbauer spectrum of the bulk interior of Kemer L4 is shown in Fig. 8. The best fit of this spectrum demonstrated the presence of three

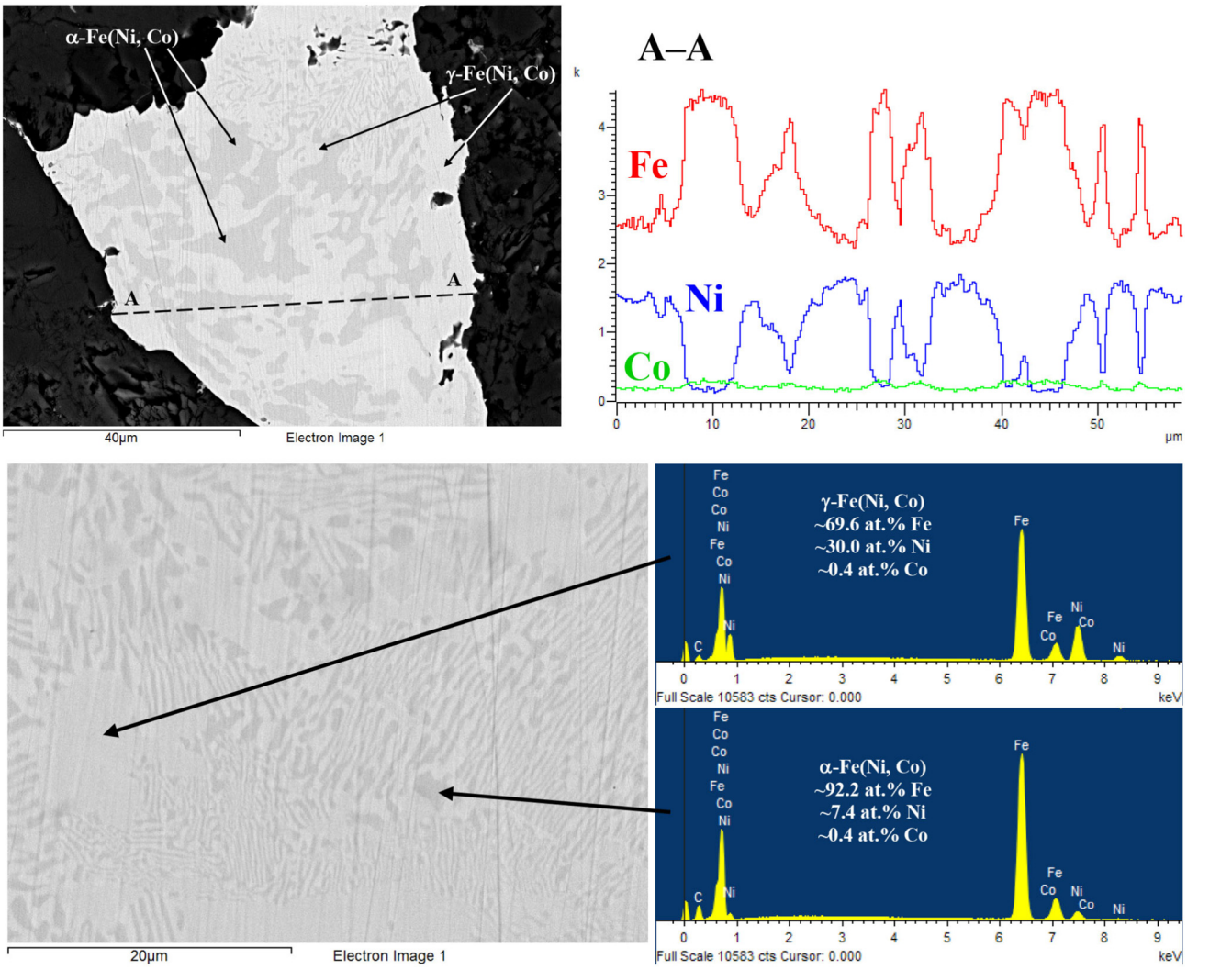

Fig. 4. Selected scanning electron microscopy images of metal grains with a complex phase composition observed in Kemer L4 polished section and taken at different magnifications with variations of Fe, Ni and Co content at the line **A**–**A** and point chemical analysis carried out using energy dispersive spectroscopy.

pairs of quadrupole doublets related to the M1 and M2 sites in olivine, orthopyroxene and clinopyroxene, respectively, three magnetic sextets assigned to the α-Fe(Ni, Co) and γ-Fe(Ni, Co) phases, one magnetic sextet related to troilite, one paramagnetic singlet associated with chromite, and two quadrupole doublets assigned to hercynite and a ferric compound. Mössbauer parameters are presented in Table 2. The ^{57}Fe hyperfine parameters obtained for the spectral components in Kemer L4 are in agreement with data for ordinary chondrites previously measured with Mössbauer spectroscopy with a high velocity resolution (see [20–23,30]). Room temperature Mössbauer parameters for the ferric compound are similar to paramagnetic FeOOH polymorphs such as ferrihydrite $5Fe_2O_3{\times}9H_2O$, akaganéite β-FeOOH, *etc.* (see, *e.g.* [31]). Taken into account the result of XRD, we can assign this component to ferrihydrite resulting from Kemer L4 weathering in terrestrial conditions.

3.2. The fusion crust

Scanning electron microscopy images at different magnifications of the Kemer L4 fusion crust are shown in Fig. 9. A formation of silicate crystals in the form of fractals from the surface melt is clearly seen. The XRD pattern of the powdered fusion crust from Kemer L4 is presented in Fig. 10. Using the Rietveld analysis, the main and minor phases were determined. The fusion crust contains 59.8 wt% olivine (ICDD 01-080-1630), 13.2 wt% orthopyroxene (ICDD 01-083-0666), 12.3 wt% magnesioferrite $MgFe_2O_4$ (ICDD 01-088-1938), 4.9 wt% Ca-rich clinopyroxene (ICDD 01-083-0088), 4.6 wt% anorthite (ICDD 01-079-1149), 2.8 wt% α-Fe(Ni, Co) phase (ICDD 00-037-0474), 1.3 wt% troilite (ICDD 01-080-1030), 0.4 wt% chromite (ICDD 00-034-0140), 0.2 wt% hercynite (ICDD 00-034-0192) and 0.4 wt% ferrihydrite (ICDD 00-046-1315). XRD observation of magnesioferrite in the fusion crust of ordinary chondrites, instead of magnetite Fe_3O_4 or wüstite FeO as shown in [2], was earlier demonstrated for Saratov L4 [32], Chelyabinsk LL5 [22] and Ozerki L6 [23]. Using the Rietveld full profile analysis, the unit cell parameters in silicate crystals in the fusion crust of Kemer L4 were determined: $a = 10.262(2)$ Å, $b = 6.006(1)$ Å, $c = 4.772(1)$ Å for olivine, $a = 18.291(4)$ Å, $b = 8.872(4)$ Å, $c = 5.191(3)$ Å for orthopyroxene, and $a = 9.72(2)$ Å, $b = 8.90(1)$ Å, $c = 5.27(1)$ Å, $\beta = 106.2°$ for Ca-rich clinopyroxene. It is interesting to point out that the unit cell parameters *a* and *b* for orthopyroxene crystals in the fusion crust appear to be slightly higher beyond the error from those in the bulk interior of Kemer L4, while the other unit cell parameters for silicate crystals are the same. This fact may indicate some redistribution of the Fe^{2+} and Mg^{2+} cations among the M1 and M2 sites in orthopyroxene crystals resulting from different thermal effects on different silicate crystals during the fusion crust formation when meteorite fell in the atmosphere.

Fig. 11 presents the magnetic behavior of the fusion crust of Kemer L4. Qualitatively speaking, the two bulk and fusion crust materials

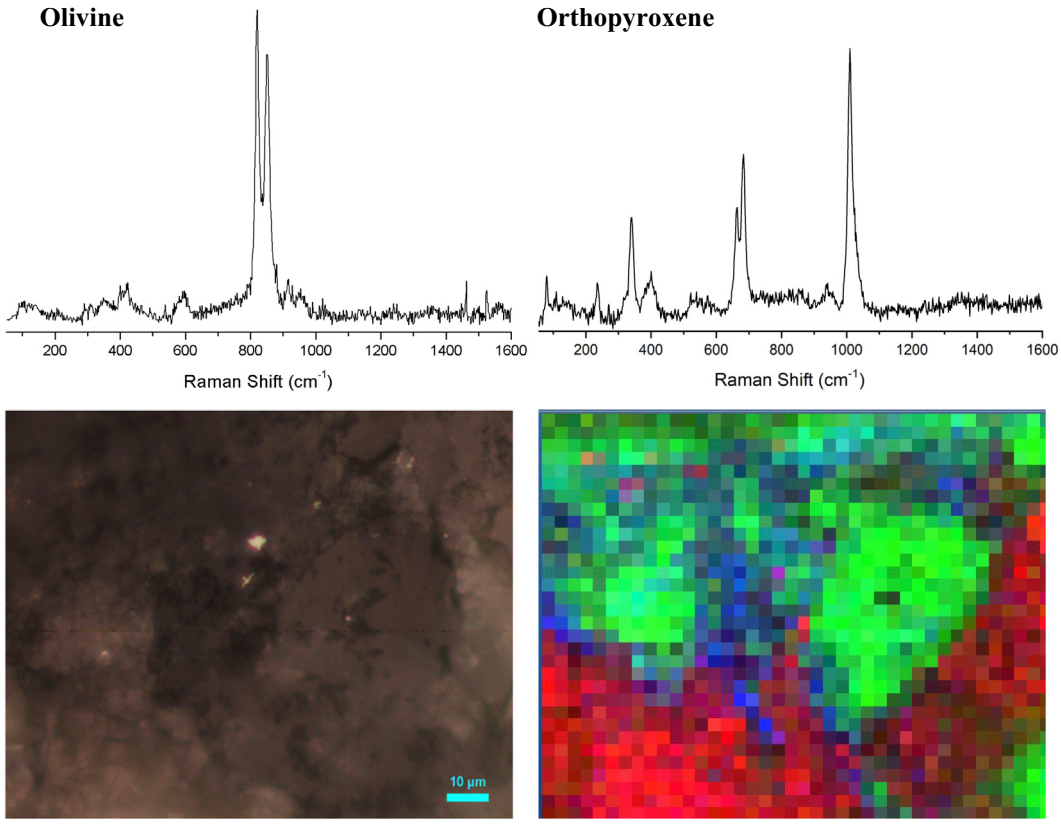

Fig. 5. Top: Representative Raman spectra for olivine and orthopyroxene in Kemer L4 polished section. Bottom: Optical image of a selected area of the silicate matrix in Kemer L4 meteorite (left) and the corresponding Raman mapping, with indication of olivine (green) and orthopyroxene (red) rich areas distribution (right). The scale in both optical and Raman mapping images is the same.

show similar magnetic behavior (see Fig. 7). From Fig. 11 it is clear that the transition at 41 K (appearing as two peaks in Fig. 7) is due to the ferrimagnetic-paramagnetic phase transition in chromite [29]. The ZFC and FC curves do not merge at 295 K, indicating a higher temperature magnetic phase transition. The $M(H)$ plots are also very similar. The curve at 5 K is composed of two major components and the $M(H)$ data are treated as above. M_S values deduced are: 21.5 and 16.2 emu/g, for 5 and 300 K, respectively. In addition, in contrast to Fig. 7, a small coercive field 110(10) and 75(10) Oe is observed at 5 and 300 K, respectively. That means that the magnetic phase fraction content in the fusion crust is much lower (and may be different) than that of the bulk interior in Kemer L4. Both internal and fusion crust materials may consist of the ferromagnetic Fe-Ni-Co alloy, but with tiny different contents resulting from meteorite combustion. This is in agreement with the results from XRD that demonstrated a decrease of Fe-Ni-Co alloy content in the fusion crust (2.8 wt%) in comparison with that in the bulk interior of the meteorite (5.6 wt%).

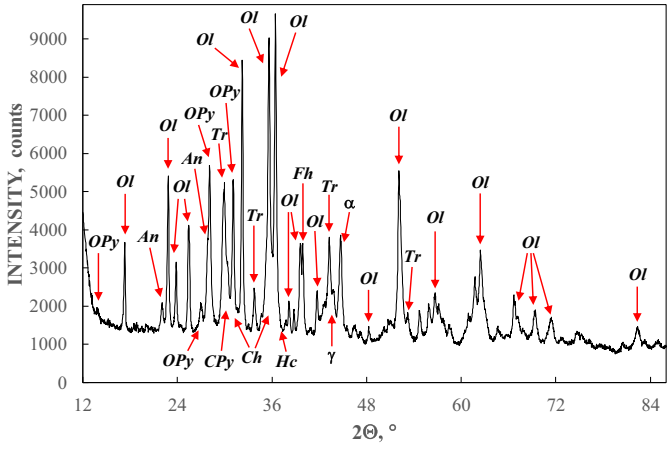

Fig. 6. X-ray diffraction pattern of the bulk interior of Kemer L4. Indicated reflexes show selected phases such as olivine (***Ol***), orthopyroxene (***OPy***), anorthite (***An***), Ca-rich clinopyroxene (***CPy***), α-Fe(Ni, Co) phase (**α**), troilite (***Tr***), γ-Fe(Ni, Co) phase (**γ**), chromite (***Ch***), hercynite (***Hc***) and ferrihydrite (***Fh***).

The Mössbauer spectrum of the fusion crust of Kemer L4 is shown in Fig. 12, with the result of the best fit and obtained components. Mössbauer parameters of these components are collected in Table 3. Using the ^{57}Fe hyperfine parameters, these components were related to the following phases and compounds: (i) two pairs of quadrupole doublets, with the largest values of ΔE_Q and δ, correspond to ferrous compounds, were assigned to the ^{57}Fe in the M1 and M2 sites in both olivine and orthopyroxene (we were unable to reveal spectral components related to the M1 and M2 sites in Ca-rich clinopyroxene due to the smaller content of this phase and the presence of other overlapping components); (ii) the fifth quadrupole doublet, with smaller ΔE_Q and δ values, that also corresponded to a ferrous compound, was associated with hercynite, while the remaining quadrupole doublet with ^{57}Fe hyperfine parameters characteristic of ferric compounds was related to ferrihydrite, as in the case of the bulk interior; (iii) one paramagnetic singlet was assigned to chromite; (iv) two magnetic sextets, with H_{eff} similar to Fe-Ni-Co alloy, were related to the α-Fe(Ni, Co) phase with at least two variations in Ni content; the total relative area of Fe-Ni-Co alloy spectral component was ~16%, while that in the bulk interior was ~22%, this decrease in the metal content in the fusion crust agreeing with the XRD and magnetization data considered above; (v) a magnetic sextet with the smallest value of H_{eff} was associated with troilite; (vi) a magnetic sextet, with the largest value of H_{eff}, was considered as indicating the formation of maghemite γ-Fe_2O_3 (see [31]); and (vii) the other four magnetic sextets were related to magnesioferrite with

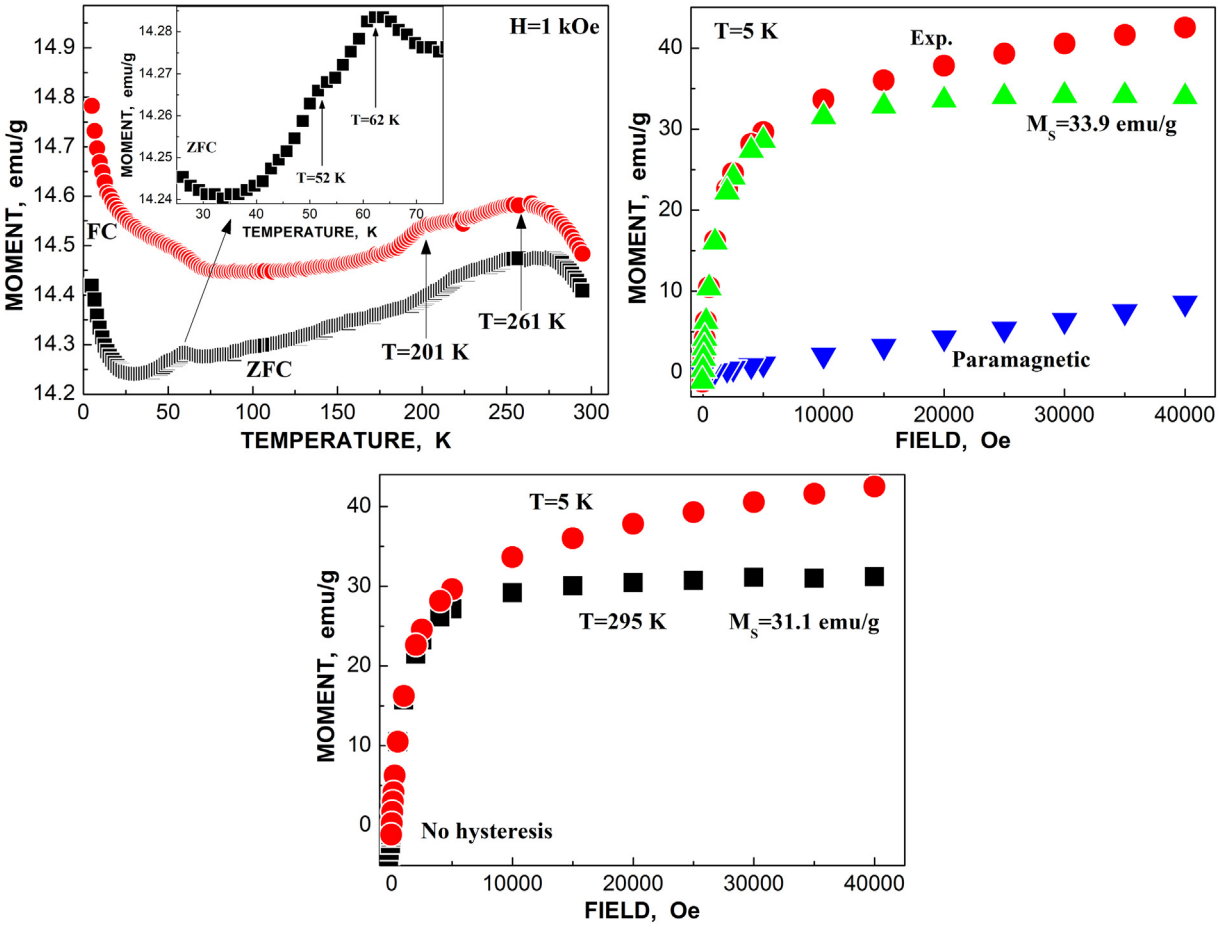

Fig. 7. Zero-field-cooled (**ZFC**) and field-cooled (**FC**) curves and isothermal magnetization curves of the bulk interior of Kemer L4. **Exp.** is experimental points, $\mathbf{M_S}$ is the saturation magnetic moment, **H** is magnetic field, **T** is temperature.

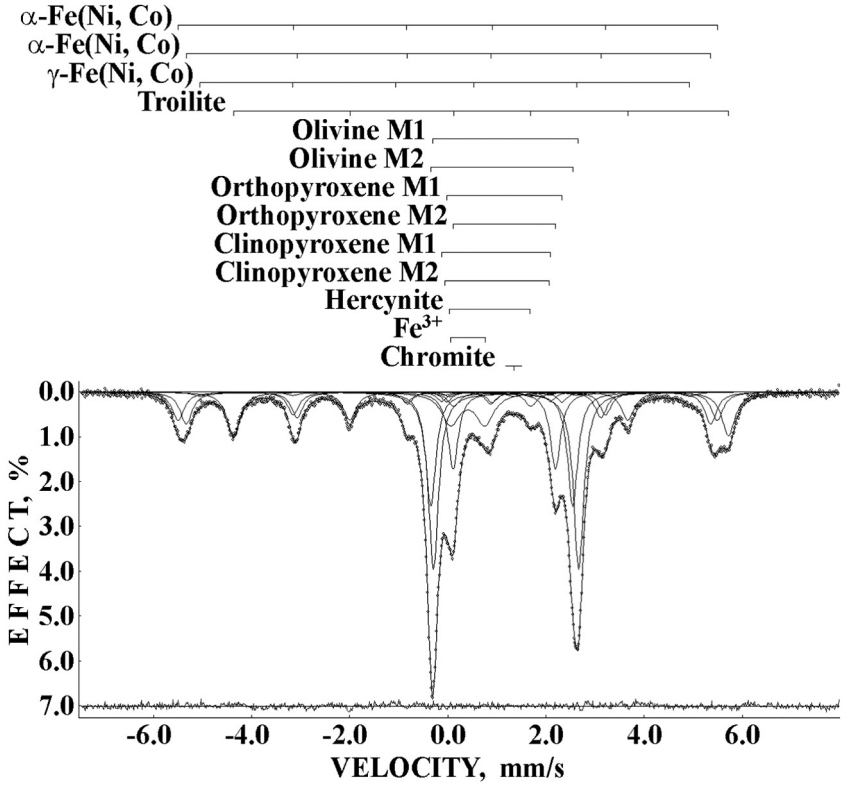

Fig. 8. Mössbauer spectrum of the bulk interior of Kemer L4. Indicated components are the result of the best fit. The differential spectrum is shown at the bottom.

Table 2
Mössbauer parameters of the bulk interior of Kemer L4.

Γ, mm/s	δ, mm/s	$\Delta E_Q/2\varepsilon$, mm/s	H_{eff}, kOe	A, %	Component
0.296 ± 0.030	0.013 ± 0.015	−0.037 ± 0.015	341.4 ± 0.5	9.66	α-Fe(Ni, Co)
0.296 ± 0.030	0.017 ± 0.015	−0.013 ± 0.015	332.1 ± 0.5	10.90	α-Fe(Ni, Co)
0.354 ± 0.042	−0.169 ± 0.015	0.203 ± 0.031	310.0 ± 0.9	1.72	γ-Fe(Ni, Co)
0.327 ± 0.030	0.763 ± 0.015	*Not determined*	313.4 ± 0.5	15.01	Troilite
0.251 ± 0.030	1.186 ± 0.015	2.961 ± 0.015	–	24.42	Olivine M1
0.251 ± 0.030	1.098 ± 0.015	2.892 ± 0.015	–	15.77	Olivine M2
0.251 ± 0.030	1.152 ± 0.018	2.346 ± 0.015	–	1.37	Orthopyroxene M1
0.251 ± 0.030	1.151 ± 0.015	2.089 ± 0.015	–	10.60	Orthopyroxene M2
0.251 ± 0.030	0.982 ± 0.016	2.215 ± 0.034	–	1.30	Clinopyroxene M1
0.251 ± 0.030	1.004 ± 0.052	2.121 ± 0.118	–	0.43	Clinopyroxene M2
0.251 ± 0.030	0.855 ± 0.039	1.645 ± 0.106	–	0.65	Hercynite
0.442 ± 0.030	0.406 ± 0.015	0.696 ± 0.019	–	7.63	Fe^{3+}
0.444 ± 0.079	1.361 ± 0.027	–	–	0.54	Chromite

different local ^{57}Fe microenvironments in the tetrahedral (A) and octahedral [B] sites in inverse spinel $(Mg_{1-x}Fe_x)_A[Mg_xFe_{2-x}]_BO_4$ with inversion parameter *x*; the values of δ are smaller for the (A) sites than for the [B] sites, therefore two sextets with δ around 0.3 mm/s were assigned to the ^{57}Fe in the tetrahedral positions while two sextets with δ around 0.8 mm/s were related to the ^{57}Fe in the octahedral positions. These assignments of spectral components are in agreement with previously studied fusion crust in Chelyabinsk LL5 and Ozerki L6 ordinary chondrites [22,23]. Some small variations in the ^{57}Fe hyperfine parameters for magnesioferrite in the fusion crust of these ordinary chondrites may be related to different Mg content and inversion parameter *x*.

XRD data showed some differences in the unit cell parameters for orthopyroxene in the bulk interior and in the fusion crust of Kemer L4, while those for olivine are the same. Therefore, it is interesting to compare these results with the ^{57}Fe hyperfine parameters for olivine and orthopyroxene in the bulk interior and in the fusion crust of Kemer L4. A comparison of Mössbauer hyperfine parameters for the ^{57}Fe in the M1 and M2 sites in olivine and orthopyroxene in the bulk interior and in the fusion crust of Kemer L4 is shown in Fig. 13. There are no differences between both M1 and M2 sites in olivine in the bulk interior and in the fusion crust. In contrast, there are clear differences in both ΔE_Q and δ values for the ^{57}Fe in the M1 sites in orthopyroxene in the bulk interior and in the fusion crust, indicating some variations in the local ^{57}Fe microenvironment of the M1 sites in these samples.

3.3. Fe^{2+} partitioning among the M1 and M2 sites in silicate crystals

The Fe^{2+} occupancies of the M1 and M2 sites (X_{Fe}^{M1} and X_{Fe}^{M2}) in olivine, orthopyroxene and clinopyroxene in the bulk interior of Kemer L4 were estimated directly from the XRD data using the approach described in [22] and references therein. Following this approach, we calculated the X_{Fe}^{M1} and X_{Fe}^{M2} values for silicate crystals, which were found to be 0.28 and 0.18 for olivine, 0.06 and 0.40 for orthopyroxene, and 0.18 and 0.06 for Ca-rich clinopyroxene.

It is also possible to estimate the ratios of the Fe^{2+} occupancies of the M1 and M2 sites in silicate crystals by analysis of the Mössbauer parameters, suggesting the same *f*-factor for all phases, as the ratios of A^{M1} and

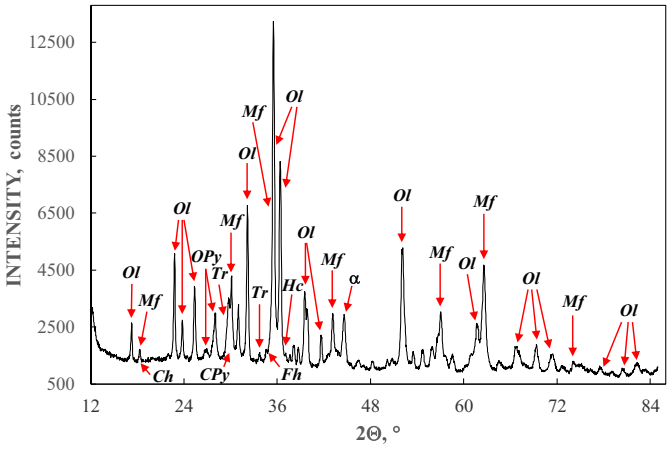

Fig. 10. X-ray diffraction pattern of the fusion crust of Kemer L4. Indicated reflexes show selected phases such as olivine (***Ol***), orthopyroxene (***OPy***), Ca-rich clinopyroxene (***CPy***), α-Fe(Ni, Co) phase (**α**), troilite (***Tr***), chromite (***Ch***), hercynite (***Hc***), ferrihydrite (***Fh***) and magnesioferrite (***Mf***).

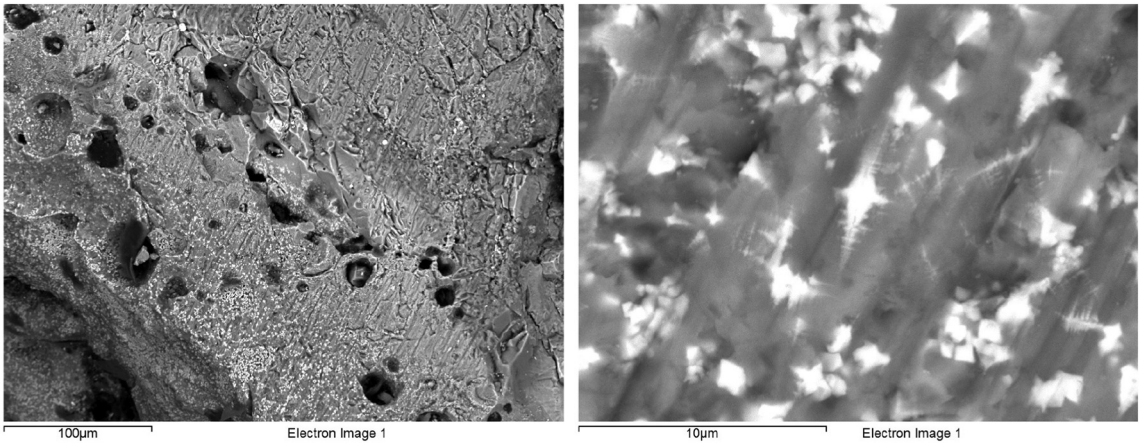

Fig. 9. Scanning electron microscopy image of the fusion crust fragment in Kemer L4 and enlarged image with silicate crystals in the form of fractals resulting from solidification of the surface melt.

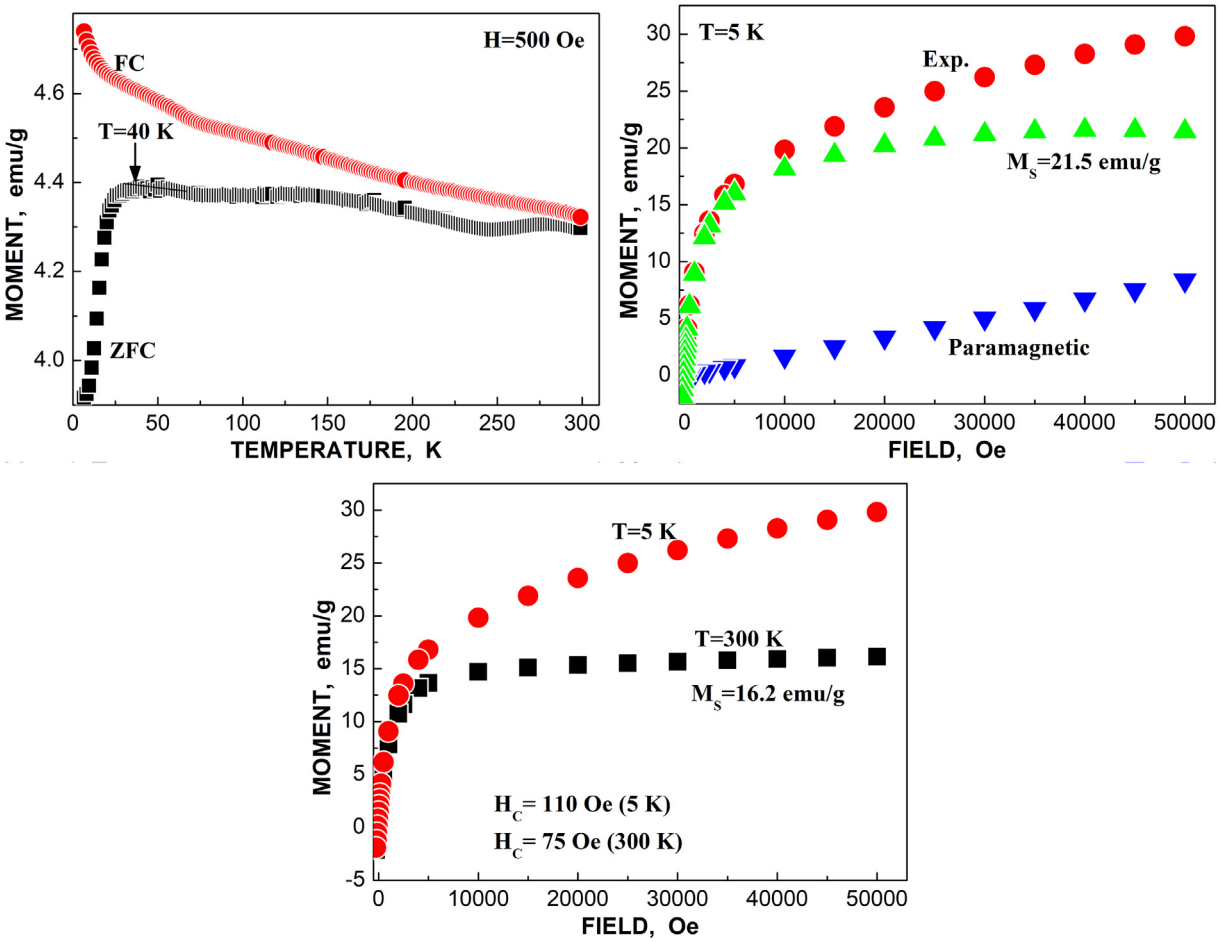

Fig. 11. Zero-field-cooled (ZFC) and field-cooled (FC) curves and isothermal magnetization curves of the fusion crust of Kemer L4. **Exp.** is experimental points, $\mathbf{M_S}$ is the saturation magnetic moment, **H** is the magnetic field, $\mathbf{H_C}$ is the coercive field, **T** is temperature.

A^{M2} for the corresponding spectral components. We can then compare the X_{Fe}^{M1}/X_{Fe}^{M2} and A^{M1}/A^{M2} ratios for silicate crystals obtained by means of two independent techniques. The obtained X_{Fe}^{M1}/X_{Fe}^{M2} and A^{M1}/A^{M2} ratios were the following: 1.56 (XRD) and 1.55 (Mössbauer spectroscopy) for olivine, 0.15 (XRD) and 0.13 (Mössbauer spectroscopy) for orthopyroxene and 3.00 (XRD) and 3.02 (Mössbauer spectroscopy) for Ca-rich clinopyroxene. Furthermore, we can also evaluate the distribution coefficient $K_D = (X_{Fe}^{M1} \times (1 - X_{Fe}^{M2})) / (X_{Fe}^{M2} \times (1 - X_{Fe}^{M1}))$ and the temperature of equilibrium cation distribution T_{eq} for Fe^{2+} and Mg^{2+} cations among the M1 and M2 sites in olivine: $-\Delta G^\circ = R \times T_{eq} \times \ln K_D$, where the Gibbs energy $\Delta G^\circ = 20{,}935$ J for olivine, and $R = 8.31$ J/K mol, following [33], and in orthopyroxene: $\ln K_D = 0.391 - 2205 / T_{eq}$, following [34] (from XRD data). To calculate these values using Mössbauer data, Fa and Fs values have to be used (for details see [22,35]). Using the data obtained by the two different techniques, calculations yielded $K_D = 1.77$, $T_{eq} = 441$ K (XRD), and $K_D = 1.77$, $T_{eq} = 439$ K (Mössbauer spectroscopy) for olivine, and $K_D = 0.10$, $T_{eq} = 806$ K (XRD) and $K_D = 0.09$, $T_{eq} = 787$ K (Mössbauer spectroscopy) for orthopyroxene. All these results, which were obtained using data from two independent techniques, are in a good agreement.

Following the approach applied recently for the fusion crust in Ozerki L6 ordinary chondrite [23] and Sariçiçek howardite [36], one could estimate the closure temperatures of Fe^{2+} and Mg^{2+} cations exchange among the M1 and M2 sites in olivine and orthopyroxene in the fusion crust of Kemer L4, with solidification and fast cooling rates (T_{FC}). The values of X_{Fe}^{M1} and X_{Fe}^{M2} determined from the XRD data are, respectively, 0.28 and 0.19 for olivine, and 0.07 and 0.37 for orthopyroxene. The X_{Fe}^{M1}/X_{Fe}^{M2} and A^{M1}/A^{M2} ratios are 1.47 and 1.53, respectively, for olivine, and 0.19 and 0.14, respectively, for orthopyroxene. Finally, using the data from the two techniques we obtained $K_D = 1.66$, $T_{FC} = 498$ K (XRD) and $K_D = 1.75$, $T_{FC} = 451$ K (Mössbauer spectroscopy) for olivine, and $K_D = 0.13$, $T_{FC} = 901$ K (XRD) and $K_D = 0.09$, $T_{FC} = 803$ K (Mössbauer spectroscopy) for orthopyroxene. These temperatures are very similar to those obtained for the meteorite bulk interior silicate phases.

4. Conclusion

A fragment of Kemer L4 ordinary chondrite was studied for the first time using optical microscopy, scanning electron microscopy with energy dispersive spectroscopy, Raman spectroscopy, X-ray diffraction, magnetization measurements, and Mössbauer spectroscopy with a high velocity resolution. The main and minor iron-bearing crystals in the bulk interior of Kemer L4, such as olivine, orthopyroxene, Ca-rich clinopyroxene, troilite, α-Fe(Ni, Co) and γ-Fe(Ni, Co) phases, chromite, hercynite, and also ferrihydrite (which is the result of meteorite terrestrial weathering), were identified using these techniques. XRD and Mössbauer spectroscopy data were used for the estimation of the Fe^{2+} occupancies in the M1 and M2 sites in olivine, orthopyroxene and Ca-rich clinopyroxene. The obtained results demonstrate a good consistency between the two independent techniques. The distribution coefficients and the temperatures of cation equilibrium distribution for olivine and orthopyroxene in Kemer L4 were also evaluated using these two techniques, which are also in a good agreement. The values of T_{eq} were around 440 K for olivine and around 800 K for orthopyroxene. This indicates a very slow cooling rate of Kemer L4, without reheating and fast cooling. This is in agreement

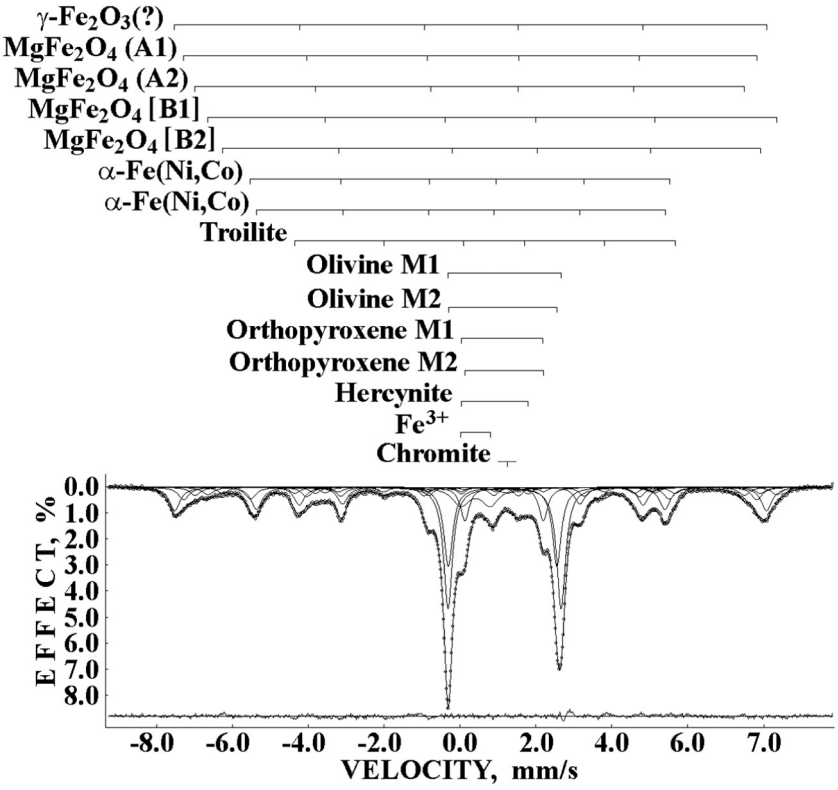

Fig. 12. Mössbauer spectrum of the fusion crust of Kemer L4. Indicated components are the result of the best fit. The differential spectrum is shown at the bottom.

Table 3
Mössbauer parameters of the fusion crust of Kemer L4.

Γ, mm/s	δ, mm/s	$\Delta E_Q/2\varepsilon$, mm/s	H_{eff}, kOe	*A*, %	Component
0.340 ± 0.038	0.287 ± 0.019	−0.015 ± 0.019	484.6 ± 0.5	11.07	γ-Fe_2O_3 (?)
0.340 ± 0.038	0.305 ± 0.019	−0.076 ± 0.019	469.2 ± 0.5	3.25	$MgFe_2O_4$ (A1)
0.340 ± 0.038	0.318 ± 0.019	−0.127 ± 0.019	449.5 ± 0.5	3.84	$MgFe_2O_4$ (A2)
0.340 ± 0.038	0.822 ± 0.019	0.056 ± 0.019	465.7 ± 0.5	3.53	$MgFe_2O_4$ [B1]
0.340 ± 0.038	0.865 ± 0.019	−0.084 ± 0.019	440.2 ± 0.6	2.88	$MgFe_2O_4$ [B2]
0.340 ± 0.038	0.029 ± 0.019	−0.071 ± 0.019	343.2 ± 0.5	5.64	α-Fe(Ni,Co)
0.340 ± 0.038	0.025 ± 0.019	−0.011 ± 0.019	334.6 ± 0.5	10.52	α-Fe(Ni,Co)
0.340 ± 0.038	0.778 ± 0.019	−0.229 ± 0.019	311.3 ± 0.5	2.90	Troilite
0.276 ± 0.038	1.171 ± 0.019	2.976 ± 0.019	–	22.74	Olivine M1
0.276 ± 0.038	1.118 ± 0.019	2.860 ± 0.019	–	14.86	Olivine M2
0.276 ± 0.038	1.104 ± 0.019	2.161 ± 0.019	–	0.87	Orthopyroxene M1
0.276 ± 0.038	1.159 ± 0.019	2.066 ± 0.019	–	6.26	Orthopyroxene M2
0.276 ± 0.038	0.909 ± 0.019	1.761 ± 0.019	–	1.28	Hercynite
0.530 ± 0.038	0.405 ± 0.019	0.774 ± 0.019	–	6.35	Fe^{3+}
0.667 ± 0.060	1.253 ± 0.026	–	–	1.32	Chromite

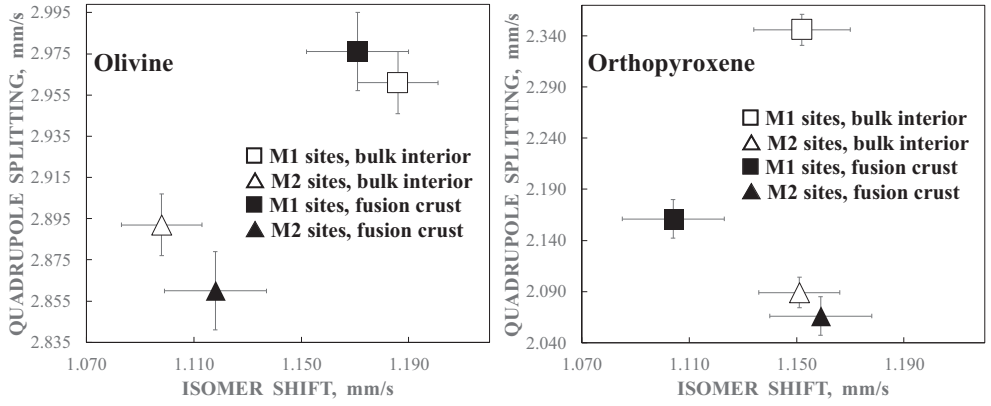

Fig. 13. Comparison of Mössbauer hyperfine parameters for the ^{57}Fe in the M1 and M2 sites in olivine and orthopyroxene in the bulk interior and in the fusion crust of Kemer L4.

with the observed troilite-metal fine-grained texture and fine intergrowings of α-Fe(Ni, Co) and γ-Fe(Ni, Co) phases, which cannot be observed after reheating and fast cooling.

The fusion crust from Kemer L4 was also studied using X-ray diffraction, magnetization measurements and Mössbauer spectroscopy with a high velocity resolution. In addition to the crystals observed in the bulk interior, we found magnesioferrite and, probably, maghemite in the meteorite fusion crust. The unit cell parameters for orthopyroxene were found slightly different in the fusion crust, compared to the bulk interior. The Fe^{2+} occupancies in the M1 and M2 sites in olivine and orthopyroxene in the fusion crust were estimated from the XRD and Mössbauer data and demonstrated a good agreement. The closure temperatures for olivine and orthopyroxene in the fusion crust were similar with T_{eq} for these crystals in the bulk interior.

CRediT authorship contribution statement

A.A. Maksimova: Investigation, Methodology, Formal analysis, Writing - original draft, Resources. **E.V. Petrova:** Investigation, Methodology, Formal analysis, Data curation, Resources. **A.V. Chukin:** Investigation, Methodology, Formal analysis, Writing - original draft. **M.S. Karabanalov:** Investigation, Methodology. **B.A. Nogueira:** Investigation, Validation. **R. Fausto:** Formal analysis, Writing - original draft. **M. Yesiltas:** Investigation, Writing - original draft. **I. Felner:** Investigation, Formal analysis, Writing - original draft, Data curation. **M.I. Oshtrakh:** Supervision, Investigation, Writing - original draft, Data curation, Writing - review & editing.

Declaration of competing interest

The authors have no conflict of interest.

Acknowledgements

The authors are grateful to Prof. Mehmet Emin Özel (Cukurova University, Adana, Turkey) and the Turkish Meteorite Working Group for providing the meteorite sample. This work was supported by the Ministry of Science and Higher Education of the Russian Federation, project № FEUZ-2020-0060, and Act 211 of the Government of the Russian Federation, contract № 02.A03.21.0006. The Coimbra Chemistry Centre (CQC; research unit UI0313/QUI/2020) is supported by the Portuguese Science Foundation (FCT) and COMPETE-UE. This work was carried out within the Agreement of Cooperation between the Ural Federal University (Ekaterinburg) and the University of Coimbra (Coimbra).

References

[1] M.K. Weisberg, T.J. McCoy, A.N. Krot, Systematics and evaluation of meteorite classification, in: D.S. Lauretta, H.Y. McSween Jr. (Eds.), Meteorites and the Early Solar System II, The University of Arizona Press, Tucson 2006, pp. 19–52.
[2] A.E. Rubin, Mineralogy of meteorite groups, Meteor. Planet. Sci. 32 (1997) 231–247.
[3] E. Jarosewich, Chemical analyses of meteorites: a compilation of stony and iron meteorite analyses, Meteoritics 25 (1990) 323–337.
[4] T.L. Dunn, G. Cressey, H.Y. McSween Jr., T.J. McCoy, Analysis of ordinary chondrites using powder X-ray diffraction: 1. Modal mineral abundances, Meteor. Planet. Sci. 45 (2010) 123–134.
[5] T.L. Dunn, H.Y. McSween Jr., T.J. McCoy, G. Cressey, Analysis of ordinary chondrites using powder X-ray diffraction: 2. Applications to ordinary chondrite parent-body processes, Meteor. Planet. Sci. 45 (2010) 135–156.
[6] N. Imae, M. Kimura, A. Yamaguchi, H. Kojima, Primordial, thermal, and shock features of ordinary chondrites: emulating bulk X-ray diffraction using in-plane rotation of polished thin sections, Meteor. Planet. Sci. 54 (2019) 919–937.
[7] M. Miyamoto, K. Ohsumi, Micro Raman spectroscopy of olivines in L6 chondrites: evaluation of the degree of shock, Geophys. Res. Lett. 22 (1995) 437–440.
[8] L. Pittarello, K. Baert, V. Debaille, P. Claeys, Screening and classification of ordinary chondrites by Raman spectroscopy, Meteor. Planet. Sci. 50 (2015) 1718–1732.
[9] P. Rochette, L. Sagnotti, M. Bourot-Denise, G. Consolmagno, L. Folco, J. Gattacceca, M.L. Osete, L. Pesonen, Magnetic classification of stony meteorites: 1. Ordinary chondrites, Meteor. Planet. Sci. 38 (2003) 251–268.
[10] A.A. Maksimova, M.I. Oshtrakh, Ordinary chondrites: what can we learn using Mössbauer spectroscopy? J. Mol. Struct. 1186 (2019) 104–117.
[11] A.A. Maksimova, A.V. Chukin, I. Felner, M.I. Oshtrakh, Spinels in meteorites: observation using Mössbauer spectroscopy, Minerals 9 (2019) 42.
[12] R.J. Hill, C.J. Howard, A computer program for Rietveld analysis of fixed wavelength X-ray and neutron diffraction patterns, Australian Atomic Energy Commission Research Report, M112, , 1986.
[13] M.I. Oshtrakh, V.A. Semionkin, O.B. Milder, E.G. Novikov, Mössbauer spectroscopy with high velocity resolution: an increase of analytical possibilities in biomedical research, J. Radioanal. Nucl. Chem. 281 (2009) 63–67.
[14] V.A. Semionkin, M.I. Oshtrakh, O.B. Milder, E.G. Novikov, A high velocity resolution Mössbauer spectrometric system for biomedical research, Bull. Rus. Acad. Sci.: Phys. 74 (2010) 416–420.
[15] M.I. Oshtrakh, V.A. Semionkin, Mössbauer spectroscopy with a high velocity resolution: advances in biomedical, pharmaceutical, cosmochemical and nanotechnological research, Spectrochim. Acta, Part A: Mol. Biomol. Spectrosc. 100 (2013) 78–87.
[16] M.I. Oshtrakh, V.A. Semionkin, Mössbauer spectroscopy with a high velocity resolution: principles and applications, in: J. Tuček, M. Miglierini (Eds.), Proceedings of the International Conference "Mössbauer Spectroscopy in Materials Science 2016", AIP Conference Proceedings, 1781, AIP Publishing, Melville, New York, 2016, 020019. .
[17] A.A. Maksimova, M.I. Oshtrakh, Z. Klencsár, E.V. Petrova, V.I. Grokhovsky, E. Kuzmann, Z. Homonnay, V.A. Semionkin, A comparative study of troilite in bulk ordinary chondrites Farmington L5, Tsarev L5 and Chelyabinsk LL5 using Mössbauer spectroscopy with a high velocity resolution, J. Mol. Struct. 1073 (2014) 196–201.
[18] M.I. Oshtrakh, A.A. Maksimova, Z. Klencsár, E.V. Petrova, V.I. Grokhovsky, E. Kuzmann, Z. Homonnay, V.A. Semionkin, Study of Chelyabinsk LL5 meteorite fragments with different lithology using Mössbauer spectroscopy with a high velocity resolution, J. Radioanal. Nucl. Chem. 308 (2016) 1103–1111.
[19] A.A. Maksimova, Z. Klencsár, M.I. Oshtrakh, E.V. Petrova, V.I. Grokhovsky, E. Kuzmann, Z. Homonnay, V.A. Semionkin, Mössbauer parameters of ordinary chondrites influenced by the fit accuracy of the troilite component: an example of Chelyabinsk LL5 meteorite, Hyperfine Interact. 237 (2016) 33.
[20] A.A. Maksimova, M.I. Oshtrakh, E.V. Petrova, V.I. Grokhovsky, V.A. Semionkin, Comparison of iron-bearing minerals in ordinary chondrites from H, L and LL groups using Mössbauer spectroscopy with a high velocity resolution, Spectrochim. Acta A Mol. Biomol. Spectrosc. 172 (2017) 65–76.
[21] A.A. Maksimova, M.I. Oshtrakh, A.V. Chukin, I. Felner, G.A. Yakovlev, V.A. Semionkin, Characterization of Northwest Africa 6286 and 7857 ordinary chondrites using X-ray diffraction, magnetization measurements and Mössbauer spectroscopy, Spectrochim. Acta A Mol. Biomol. Spectrosc. 192 (2018) 275–284.
[22] M.I. Oshtrakh, A.A. Maksimova, A.V. Chukin, E.V. Petrova, P. Jenniskens, E. Kuzmann, V.I. Grokhovsky, Z. Homonnay, V.A. Semionkin, Variability of Chelyabinsk meteoroid stones studied by Mössbauer spectroscopy and X-ray diffraction, Spectrochim. Acta A Mol. Biomol. Spectrosc. 219 (2019) 206–224.
[23] A.A. Maksimova, E.V. Petrova, A.V. Chukin, M.S. Karabanalov, I. Felner, M. Gritsevich, M.I. Oshtrakh, Characterization of the matrix and fusion crust of the recent meteorite fall Ozerki L6, Meteor. Planet. Sci. 55 (2020) 231–244.
[24] M.I. Oshtrakh, A.A. Maksimova, M.V. Goryunov, E.V. Petrova, I. Felner, A.V. Chukin, V.I. Grokhovsky, Study of metallic Fe-Ni-Co alloy and stony part isolated from Seymchan meteorite using X-ray diffraction, magnetization measurement and Mössbauer spectroscopy, J. Mol. Struct. 1174 (2018) 112–121.
[25] A. Chopelas, Single crystal Raman spectra of forsterite, fayalite, and monticellite, Am. Mineral. 76 (1991) 1101–1109.
[26] K. Mohanan, S.K. Sharma, F.C. Bishop, A Raman spectral study of forsterite-monticellite solid solutions, Am. Mineral. 78 (1993) 42–48.
[27] T. Mouri, M. Enami, Raman spectroscopic study of olivine-group minerals, J. Mineral. Petrol. Sci. 103 (2008) 100–104.
[28] E. Huang, C.H. Chen, T. Huang, E.H. Lin, J. Xu, Raman spectroscopic characteristics of Mg-Fe-Ca pyroxenes, Am. Mineral. 85 (2000) 473–479.
[29] J. Gattacceca, P. Rochette, F. Lagroix, P.-E. Mathé, B. Zanda, Low temperature magnetic transition of chromite in ordinary chondrites, Geophys. Res. Lett. 38 (2011), L10203.
[30] T. Kohout, J. Haloda, P. Halodová, M.M.M. Meier, C. Maden, H. Busemann, M. Laubenstein, M.W. Caffee, K.C. Welten, J. Hopp, M. Trieloff, R.R. Mahajan, S. Naik, J.M. Trigo-Rodriguez, C.E. Moyano-Cambero, M.I. Oshtrakh, A.A. Maksimova, A.V. Chukin, V.A. Semionkin, M.S. Karabanalov, I. Felner, E.V. Petrova, E.V. Brusnitsyna, V.I. Grokhovsky, G.A. Yakovlev, M. Gritsevich, E. Lyytinen, J. Moilanen, N.A. Kruglikov, A.V. Ishchenko, Annama H chondrite — mineralogy, physical properties, cosmic ray exposure, and parent body history, Meteor. Planet. Sci. 52 (2017) 1525–1541.
[31] E. Murad, Mössbauer spectroscopy of clays, soils and their mineral constituents, Clay Miner. 45 (2010) 413–430.
[32] I.A. Yudin, Yu.D. Kozmanov, I.M. Remennikova, Investigation of minerals in the fusion crust of Saratov meteorite, Meteoritics (Moscow) 28 (1968) 156–157 (in Russian).
[33] T.V. Malysheva, Mössbauer Effect in Geochemistry and Cosmochemistry, Nauka, Moscow, 1975 166 (in Russian).
[34] L. Wang, N. Moon, Y. Zhang, W.R. Dunham, E.J. Essene, Fe-Mg order-disorder in orthopyroxenes, Geochim. Cosmochim. Acta 69 (2005) 5777–5788.
[35] M.I. Oshtrakh, E.V. Petrova, V.I. Grokhovsky, V.A. Semionkin, A study of ordinary chondrites by Mössbauer spectroscopy with high-velocity resolution, Meteor. Planet. Sci. 43 (2008) 941–958.
[36] A.A. Maksimova, O. Unsalan, A.V. Chukin, M.S. Karabanalov, P. Jenniskens, I. Felner, V.A. Semionkin, M.I. Oshtrakh, The interior and the fusion crust in Sariçiçek howardite: study using X-ray diffraction, magnetization measurements and Mössbauer spectroscopy, Spectrochim. Acta A Mol. Biomol. Spectrosc. 228 (2020) 117819.